DOI 10.5012/bkcs.2011.32.4.1187

Theoretical Studies on Mechanism and Kinetics of the Hydrogen-Abstraction Reaction of CF_3CH_2CHO with OH Radicals

Cheng-gang Ci, Hong-bo Yu, Su-qin Wan, Jing-yao Liu,* and Chia-Chung Sun

*State Key Laboratory of Theoretical and Computational Chemistry, Institute of Theoretical Chemistry, Jilin University, Changchun 130023, P. R. China. *E-mail: ljy121@jlu.edu.cn*
Received Octobe 5, 2010, Accepted February 2, 2011

The hydrogen abstraction reaction of CF_3CH_2CHO + OH has been studied theoretically by dual-level direct dynamics method. Two stable conformers, *trans*- and *cis*-CF_3CH_2CHO, have been located, and there are four distinct OH hydrogen-abstraction channels from *t*-CF_3CH_2CHO and two channels from *c*-CF_3CH_2CHO. The required potential energy surface information for the kinetic calculation was obtained at the MCG3-MPWB//M06-2X/aug-cc-pVDZ level. The rate constants, which were calculated using improved canonical transition-state theory with small-curvature tunneling correction (ICVT/SCT) were fitted by a four-parameter Arrhenius equation. It is shown that the reaction proceeds predominantly *via* the H-abstraction from the -CHO group over the temperature range 200-2000 K. The calculated rate constants were in good agreement with the experimental data between 263 and 358 K.

Key Words : Direct dynamics method, Rate constant, Variational transition-state theory, Density functional theory, Reaction mechanism

Introduction

Because of the well-known depletion on stratospheric ozone layer and greenhouse effects of the chlorofluorocarbons (CFCs), many concerted effects have been made to replace CFCs with environmentally acceptable substitutes. Hydrofluorocarbon (HFCs) and hydrochlorofluorpcarbons (HCFCs) are two classes of compounds which have been used as CFCs alternatives.[1-3] However, they have high contributions to global warming potential (GWP) as the results of their long atmospheric lifetimes and strong absorption in the IR region. Recently, hydrofluoroethers (HFEs) and partially fluroalchohols (FAs) (having the structure of $CF_3(CH_2)_xCH_2OH$) have been proposed as a new generation of CFCs used in many industrial applications.[4-6]

$CF_3CH_2CH_2OH$ is the one among the family of $CF_3(CH_2)_xCH_2OH$, and its major atmospheric photooxidation product is CF_3CH_2CHO.[7-10] The major degradation process of CF_3CH_2CHO in atmosphere is initiated by the OH radicals. Experimental studies have been performed by some groups to determine the absolute and relative rate constants of the CF_3CH_2CHO + OH reaction.[9-12] The rate constants (k) at room temperature reported by Kelly *et al*.,[9] Hurley *et al.*[10] and Antiñolo *et al.*[11] showed very good consistency, in the range of $(2.57 \pm 0.44) \times 10^{-12} \sim (2.96 \pm 0.04) \times 10^{-12}$ cm^3 molecule^{-1} s^{-1}, while they were slightly lower than the value of $(3.60 \pm 0.30) \times 10^{-11}$ cm^3 molecule^{-1} s^{-1}.[12] Also, Antiñolo *et al.*[11] found the rate constants exhibited a slightly positive temperature dependence between 263 and 358 K, with an estimated activation energy of about 0.62 kcal mol^{-1}. To the best of our knowledge, no other kinetic data or theoretical study is available for this reaction up to now. Thus, in order to ascertain the environmental impact of these fluorinated alcohols released into the troposphere, a mechanistic and kinetic study of the resulting secondary oxidation product CF_3CH_2CHO with OH is very desirable.

In the present work, we performed dual-level (X//Y) direct dynamics calculations[13-15] to investigate the kinetic nature of the title reaction. The required potential energy surface (PES) information for the kinetic calculations was obtained directly from the electronic structure calculations, in which the M06-2X density functional method[16] was used to optimize all the stationary points on the PES, and multilevel MCG3-MPWB method[17] was used to calculate the high-level single-point energies at the M06-2X geometries. The rate constants were evaluated using variational transition state theory (VTST)[18-20] with interpolated single-ponit energies (ISPE)[21] approach. The comparison between theoretical and experimental results is made. In addition, the enthalpies of formation of the reactant and product radicals were estimated theoretically by using isodesmic reactions.[22]

Computational Methods

The equilibrium geometries of all the stationary points including the reactants, transition states, products, and complexes were optimized by the M06-2X method with the aug-cc-pVDZ basis set (M06-2X/aug-cc-pVDZ). Normal-mode frequency analysis was performed at the same level to characterize the nature of each stationary point and to make the zero-point energy (ZPE) corrections. The local minima possess all real frequencies whereas the transition states (TS) have only one imaginary frequency. A factor of 0.9721[16] is used to scale the M06-2X/aug-cc-pVDZ frequencies. The minimum energy path (MEP) was constructed by intrinsic reaction coordinate (IRC) theory for each reaction channel.

The energy derivatives including gradients and Hessians at geometries along the MEP were obtained. To obtain more accurate energetics, the single-point energies of the stationary and nonstationary points were calculated by the multi-coefficient extrapolated density functional method MCG3-MPWB. The dual-level potential energy profile was refined using variational transition state theory with interpolated single-point energy method (VTST-ISPE). In this approach, the high-level energies of a limited number of the selected points along the reaction path are required. Moreover, the effect of basis set superposition error (BSSE) on the energies of the complexes was investigated by using the complete basis set extrapolation CBS-QB3 method.[23,24] The MCG3-MPWB calculations were carried out by using the MLGAUSS program version 2.0[25] in conjunction with the Gaussian 03 program package,[26] and the other electronic structure calculations were performed with the Gaussian 09 program package.[27]

By means of the POLYRATE 9.7 program,[28] the theoretical rate constants for each channel were calculated by improved canonical variational transition theory (ICVT) with the small-curvature tunneling (SCT) approximation.[29-31] The lower-frequency vibrational modes corresponding to the internal rotation are treated as hindered rotors, while all of the other modes are treated by quantum mechanical separable harmonic oscillators.[32,33] Two electronic states of the OH radical, with a 140 cm^{-1} splitting in the $^2\Pi$ ground state, were included in the calculation of its electronic partition function.

Since no standard enthalpies (ΔH^o_{298}) of formation of the reactant CF_3CH_2CHO and product radicals CF_3CH_2CO and CF_3CHCHO have been reported experimentally or theoretically, we employed the following isodesmic reaction I-III to estimate the ΔH^o_{298} values of these species.

$$CF_3CH_2CHO + CH_4 \rightarrow CH_3CHO + CF_3CH_3 \quad (I)$$

$$CF_3CH_2CO + CH_4 \rightarrow CH_3CO + CF_3CH_3 \quad (II)$$

$$CF_3CHCHO + CH_4 \rightarrow CH_3CHO + CF_3CH_2 \quad (III)$$

The electronic structure calculations of above three reactions involved both *trans* and *cis* conformers were also performed at the same MCG3-MPWB//M06-2X/aug-cc-pVDZ level.

Results and Discussions

Stationary Points.

Structures and Vibrational Frequencies: The optimized structures of all the stationary points at the M06-2X/aug-cc-pVDZ level are displayed in Figure 1, along with the available experimental data[34] of OH and H_2O, and the corresponding harmonic vibrational frequencies are listed in Table S1 as Supporting Information. The reactants, products and complexes have all real frequencies, and the transition

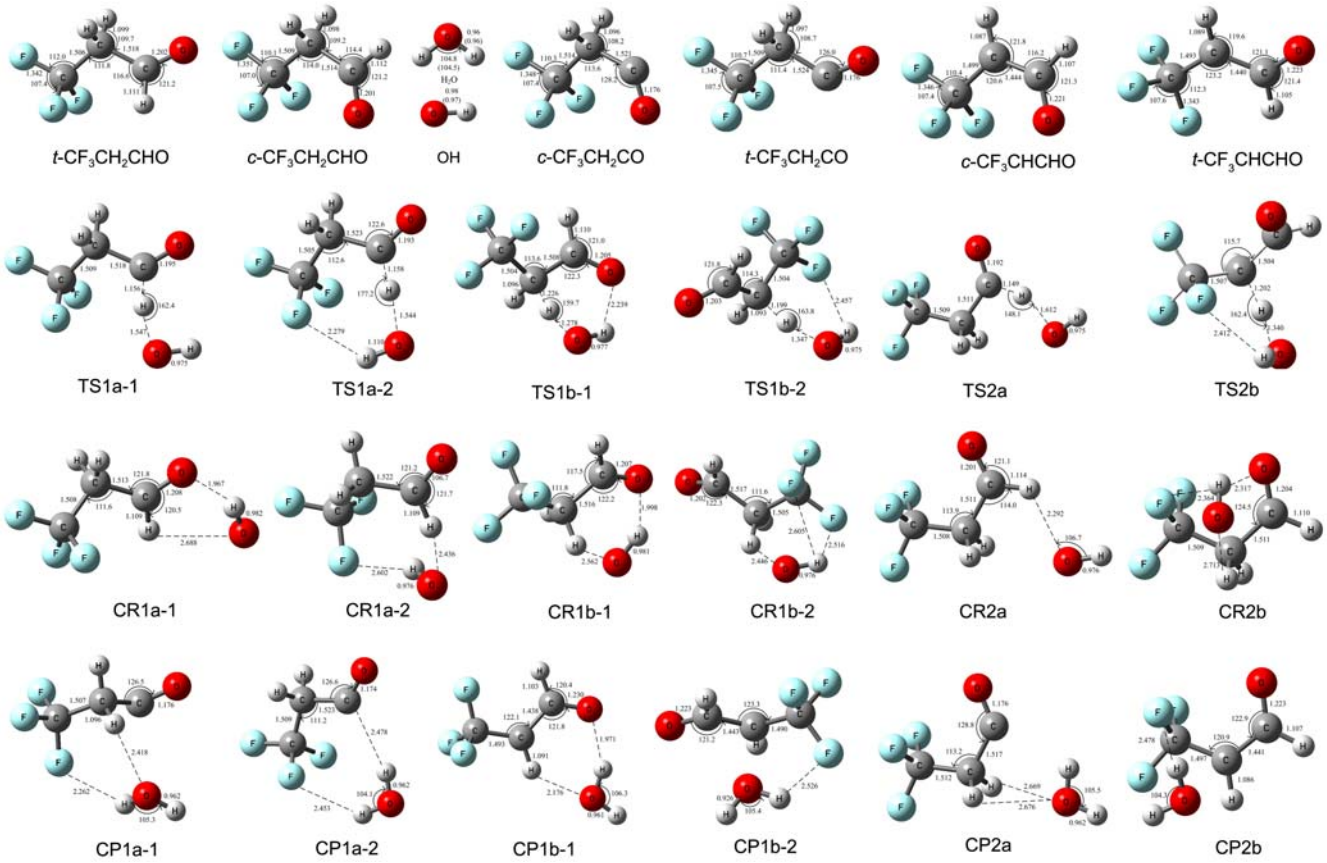

Figure 1. Optimized geometry parameters of reactants, products, transition-states, and hydrogen-bond complexes at the M06-2X/aug-cc-pVDZ. Experimental values are given in parentheses. Bond lengths are in angstroms and angles are in degree.

states are identified with only one imaginary frequency. The imaginary frequencies in the TSs correspond to the stretching modes of the coupling between the breaking and forming bonds. It is found that *trans*-CF_3CH_2CHO (denoted as *t*-CF_3CH_2CHO) and *cis*-CF_3CH_2CHO (denoted as *c*-CF_3CH_2CHO) are the two stable conformers of CF_3CH_2CHO, with the O-C-C-C dihedral angles of 149.9° and 0°, respectively, and they can transform to each other by the rotation of the -CHO group. *t*-CF_3CH_2CHO with C_1 symmetry is found to be more stable than *c*-CF_3CH_2CHO with C_s symmetry by about 1.0 kcal mol^{-1} at the M06-2X/aug-cc-pVDZ level and 1.2 kcal mol^{-1} at the MCG3-MPWB//M06-2X level. Because of the small energy difference between the two conformers, the contributions of both of them are taken into account in the kinetic calculation.

Hydrogen atom can be abstracted from the -CHO and -CH_2- groups of CF_3CH_2CHO. For *t*-CF_3CH_2CHO, two distinct H-abstraction transition states from -CHO (TS1a-1 and TS1a-2) are located based on the different attack orientations of the OH radical, and the other two (TS1b-1 and TS1b-2) from -CH_2- are found according to the inequivalent positions of the two H atoms, as shown in Figure 2(a), i.e.,

$$t\text{-}CF_3CH_2CHO + OH \rightarrow t\text{-}CF_3CH_2CO + H_2O \quad \text{(1a-1 and 1a-2)}$$

$$\rightarrow t\text{-}CF_3CHCHO + H_2O \quad \text{(1b-1 and 1b-2)}$$

While in the case of *c*-CF_3CH_2CHO, only one distinct H-abstraction channel is found from the -CHO and -CH_2- groups (see Figure 2b), respectively, that is

$$c\text{-}CF_3CH_2CHO + OH \rightarrow c\text{-}CF_3CH_2CO + H_2O \quad (2a)$$

$$\rightarrow c\text{-}CF_3CHCHO + H_2O \quad (2b)$$

For the corresponding *trans* and *cis* structures of the product radicals, the O-C-C-C dihedral angles are 180° and 0°, respectively. At the MCG3-MPWB//M06-2X level, the energy difference is 0.8 kcal mol^{-1} between *t*-CF_3CH_2CO and *c*-CF_3CH_2CO, and it is 1.6 kcal mol^{-1} between *t*-CF_3CHCHO and c-CF_3CHCHO.

Due to the high electronegativity of the fluorine and oxygen atoms, hydrogen-bonded complexes with energies lower than the reactants or products are located at the entrance or exit of each channel, indicating that the H-abstraction reaction may proceed *via* an indirect mechanism. In these complexes, the hydrogen-bond distances of O···H and H···F are all less than their van der waals radii (2.72 and 2.67 Å), and the other bond lengths are very close to those of the corresponding reactants or products. Similarly, the intramolecular hydrogen bonds between H and O or between H and F also exist in some transition states, such as TS1a-2, TS1b-1, TS1b-2, and TS2b, which have six-membered ring structures. In addition, it is seen that the geometries of TSs look more similar to those of reactants than to those of products. For example, in TS1a-1 and TS1b-1, the breaking bonds (C-H) are stretched by about 4% and 12%, respectively, compared to the C-H equilibrium bond lengths in the isolated (*c* and *t*) CF_3CH_2CHO, and the forming H-O bonds are longer than the regular bond length of H_2O by about 61% and 33%, respectively. The elongations of the forming bond are greater than the elongations of the breaking bonds, indicating that the two transition states are reactant-like, i.e., the two channels may pass through "early" transition states. Similar characters can be found in other transition states.

Energetics: The calculated reaction enthalpies (ΔH^o_{298}) of $CF_3CH_2CHO + OH \rightarrow CF_3CH_2CO + H_2O$ (R1a and R2a) are −29.7 (for trans conformer) and −29.4 kcal mol^{-1} (for *cis* conformer) at the MCG3-MPWB//M06-2X level, which are about 7 kcal mol^{-1} more exothermic than those of the H-abstract channels from the -CH_2- group (R1b and R2b). Because of lack of the experimental enthalpies ($\Delta H^o_{f,298}$) of the reactant and product radicals, a direct comparison between theoretical and experimental results is not available. Here we predict the $\Delta H^o_{f,298}$ values of both trans and cis conformers of CF_3CH_2CHO, CF_3CH_2CO, and CF_3CHCHO using isodesmic reactions I-III mentioned above. The optimization calculations of reactions I-III were performed at the M06-2X/aug-cc-pVDZ level and single-point energies were improved by MCG3-MPWB method. Then, the calculated reaction enthalpies are combined with the known standard enthalpies of formation of the reference compounds (CH_4, −17.9 kcal mol^{-1};[35] CH_3CHO, −40.8 ± 0.4 kcal mol^{-1};[35] CH_3CO, −2.9 ± 0.7 kcal mol^{-1};[35] CF_3CH_3, −178.7 ± 0.8 kcal mol^{-1};[35] and CF_3CH_2, −123.6 ± 1.0 kcal mol^{-1} [36]) to estimate the $\Delta H^o_{f,298}$ values of these species. The corresponding results are given in Table 1.

Schematic potential energy surfaces of the title reaction obtained at the MCG3-MPWB//M06-2X level with the ZPE corrections are plotted in Figure 2(a)-(b). The energy of the corresponding reactant is set to zero for reference. As can be seen from Figure 2(a), for the *t*-CF3CH2CHO + OH reaction, the pre-reactive hydrogen-bonded complexes CR1a-1, CR1a-2, CR1b-1, and CR1b-2 are firstly formed at the entrance of the four channels, with the stabilization energies of −3.6, −1.3, −3.2, and −1.4 kcal mol^{-1}, respectively. Then, starting from the reactant complex, each reaction undergoes an H-transfer process to form the products *via* a product complex. Complexes CP1a-1, CP1a-2, CP1b-1, and CP1b-2 lie 2.2, 0.4, 4.3 and 2.1 kcal mol^{-1} below the corresponding products, respectively. For reaction R1, the transition states, TS1a-1 and TS1a-2, lie lower than the reactants by about −0.5 and −1.2 kcal mol^{-1}, respectively, by the M06-2X method, and the relative energies are −0.5 and −0.9 kcal

Table 1. The standard enthalpies of formation ($\Delta H^o_{f,298}$) (in kcal·mol^{-1}) at 298 K calculated at the MCG3-MPWB//M06-2X/aug-cc-pVDZ level.

Species	$\Delta H^o_{f,298}$	Species	$\Delta H^o_{f,298}$
t-CF_3CH_2CHO	−190.6	*c*-CF_3CH_2CHO	−191.5
t-CF_3CH_2CO	−153.3	*c*-CF_3CH_2CO	−151.9
t-CF_3CHCHO	−146.1	*c*-CF_3CHCHO	−144.5

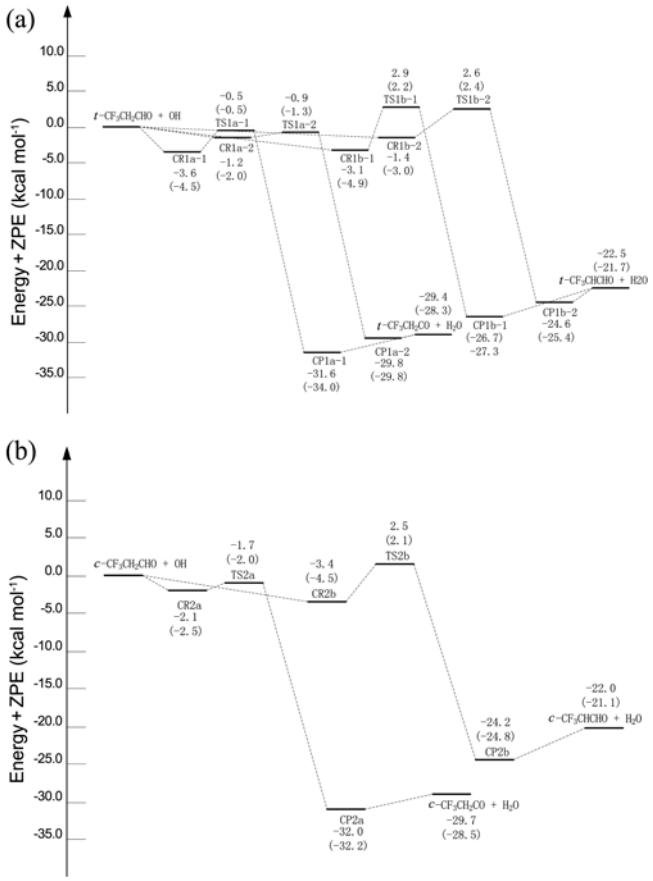

Figure 2. Schematic potential energy surfaces (a) for the *t*-CF_3CH_2CHO + OH reaction, and (b) for the *c*-CF_3CH_2CHO + OH reaction. Relative energies with ZPE at the MCG3-MPWB//M06-2X/aug-cc-pVDZ level are in kcal mol^{-1}. The values in parenthesis are those obtained at the M06-2X/aug-cc-pVDZ level.

mol^{-1}, respectively, at the MCG3-MPWB//M06-2X level. Clearly, both M06-2X and MCG3-MPWB//M06-2X calculations yield negative barriers for the H-abstraction channels (1a-1 and 1a-2) of *t*-CF_3CH_2CHO from the -CHO group. Also, it is found that TS1a-2 is slightly more stable than TS1a-1 by about 0.7 and 0.4 kcal mol^{-1} at the low- and high-level, respectively, due to the existence of the intramolecular hydrogen bonding H···F in TS1a-2. The relative energies of TS1b-1 and TS1b-2 (H-abstractions from the -CH_2- group) are 2.9 and 2.6 kcal mol^{-1} respectively, which are about 3-4 kcal mol^{-1} higher than those of TS1a-1 and TS1a-2, and these two channels R1b-1 and R1b-2 are less exothermic than channels R1a (1-2) by about 7 kcal mol^{-1}. Thus, just from the energetic point of view, it is concluded that reaction R1 may proceed predominantly through the H-abstraction channels from the -CHO group, while H-abstraction channels from the -CH_2- site are kinetically noncompetitive. Similar conclusion can be drawn for the *c*-CF_3CH_2CHO + OH reaction. Moreover, due to the fact that the basis set superposition error (BSSE) is of the same order of magnitude as binding energies of the weak hydrogen-bonded complexes, in present study, we employed the complete basis set extrapolation CBS-QB3 method to correct for BSSE for the reactant

Table 2. Binding energies (in kcal mol^{-1}) for the reactant complexes

	MCG3-MPWB// M06-2X/aug-cc-pVDZ	CBS-QB3
CR1a-1	−3.6	−3.4
CR1a-2	−1.3	−1.5
CR1b-1	−3.2	−2.7
CR1b-2	−1.4	−1.7
CR2a	−2.2	−1.5
CR2b	−3.5	−2.2

complexes. The resulting CBS-QB3 results are listed in Table 2 and compared with the MCG3-MPWB//M06-2X values. As seen in the Table 2, the binding energies obtained at the MCG3-MPWB level are close to the CBS-QB3 results, with the magnitudes of BSSE ranging from 0.2 to 1.3 kcal mol^{-1}, which indicate that the BSSE correction for these complexes may not be negligible but relatively small, and in all cases, these complexes indeed exist in the entrance valley. Thus we conclude that the well depths of all complexes evaluated at the MCG3-MPWB//M06-2X level are reliable and can be used for the kinetic calculations. In addition, it is seen that channel R2a has a more negative barrier than R1a-1 and R1a-2. The relative energy of TS2a, −1.7 kcal mol^{-1}, is lower than the relative energies of TS1a-1 and TS1a-2 by 1.2 and 0.8 kcal mol^{-1}, respectively, implying that the hydrogen abstraction from *c*-CF_3CH_2CHO (R2a) may be much faster than the corresponding H-abstraction from *t*-CF_3CH_2CHO (R1a-1 and R1a-2); as a result, although *c*-CF_3CH_2CHO is 1.2 kcal mol^{-1} higher than *t*-CF_3CH_2CHO in energy, its contribution to the whole reaction cannot be ignored.

Rate Constant Calculation. Dual-level dynamics calculations were carried out using VTST-ISPE approach at the MCG3-MPWB//M06-2X/aug-cc-pVDZ level. Figure 3(a)-(b) depicts the classical potential energy curves ($V_{MEP}(s)$), the vibrationally adiabatic ground-state potential energy curves ($V_a^G(s)$), and the ZPE curves (ZPE(s)) for reactions R1a-1, and R1b-1, respectively, where $V_a^G(s) = V_{MEP}(s) + ZPE(s)$. The curves for R1a-2, R1b-2, R2a, and R2b are displayed in Figure S1 a-d as Supporting Information. Seen from Figure 3(a), the maximum of the classical potential energy V_{MEP} evaluated at the MCG3-MPWB//M06-2X level is located at $s(V_{MEP}) = 0.225$ $(amu)^{1/2}$ bohr and has a value of −0.02 kcal mol^{-1}. When the ZPE correction is added, the maximum of adiabatic energy profile occurs at $s(V_a^G) = -0.675$ $(amu)^{1/2}$ bohr, and the adiabatic energy barrier at $s(V_a^G)$ is −0.06 kcal mol^{-1}, which is 1.14 kcal mol^{-1} higher than the value at the classical-potential-energy maximum $s(V_{MEP})$. These values indicate that the variational effect is important for this channel. Similar case can be found for the other H-abstraction channels from the −CHO group, R1a-2 and R2a. Also, the dynamic bottleneck properties of R1a-1 and R1b-1 based on the ICVT approach are listed in Table 3. In the cases of these low-barrier reactions, entropic consideration controls the locations of the generalized transition states, and this is responsible for the varational effect. Table

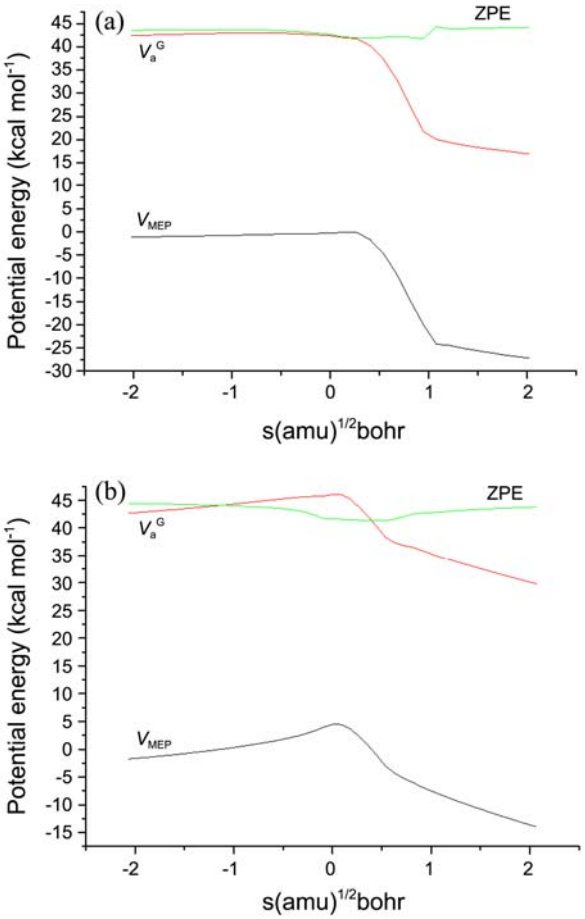

Figure 3. Classical potential energy curves (V_{MEP}), ground-state vibrationally adiabatic energy curves (V_a^G), and zero-point energy curve (ZPE) as functions of s (amu)$^{1/2}$ bohr at the MCG3-MPWB//M06-2X/aug-cc-pVDZ level: (a) for R1a-1and (b) for R1b-1.

3 shows that the variational effect is quite large at low temperatures and decreases with increasing temperature. For the H-abstraction R1b-1, from the -CH_2- group, it can be seen that the maxima of the $V_{MEP}(s)$ and $V_a^G(s)$ curves (see Figure 3b) are almost the same, and the dynamic-bottleneck locations are just slightly shifted away from the saddle point over the whole temperature range, that is, there is a negligible variational effect for R1b-1. Similar behaviors can be drawn for the H-abstraction channels, R1b-2 and R2b.

Table 3. Bottleneck properties for channels R1a-1 and R1b-1 based on ICVT calculations

T (K)	R1a-1			R1b-1		
	s [a]	V_{MEP} [b]	V_a^G [c]	s [a]	V_{MEP} [b]	V_a^G [c]
S. P.	0.000	–0.29	42.38	0.000	4.49	46.05
200	–0.695	–0.61	43.01	0.053	4.56	46.11
250	–0.770	–0.65	43.00	0.056	4.56	46.11
298	–0.793	–0.66	43.00	0.058	4.56	46.11
500	–0.812	–0.67	42.99	0.068	4.54	46.09
800	0.256	–0.08	41.80	0.078	4.52	46.06
1000	0.261	–0.10	41.80	0.084	4.50	46.03
2000	0.280	–0.21	41.67	0.100	4.43	45.96

[a]in unit of (amu)$^{1/2}$ bohr. [b]in unit of kcal mol^{-1}. [c]in unit of kcal mol^{-1}

The TST, ICVT, ICVT/SCT rate constants for channels R1a-1, R1a-2, R2a, and R1b-1 are plotted in Figure 4(a)-(d). As seen from Figure 4(a)-(c), the TST rate constants (k(TST)) show negative temperature dependence at low temperatures, below 520 K for R1a-1 and R1a-2 and below 600 K for R2a. While as discussed above, for the reactions with low, non-existent or negative energy barriers, entropy is more important than energy, consequently, adding in entropic effects leads to a larger variational effect, which makes rate constants much smaller than the TST ones. In the cases of R1a-1 and R1a-2, as a result of a slightly positive ICVT free energy caused by the variational effect, the ICVT rate constant (k(ICVT)) exhibits slightly positive temperature dependence. The case is different for R2a. The energy barrier of R2a is negative enough to produce a slightly negative free energy, so even considering the entropic contribution, the temperature dependence of the ICVT rate constant is still negative, but the Arrhenius plot of k(ICVT) presents lesser curved than the k(TST) plot. The negative temperature dependence of k(ICVT) is found below 820 K for R2a. Therefore, we concluded that the curved Arrhenius plots of k(ICVT/SCT) of channels R1a-1 and R1a-2 are entirely due to a significant variational effect, which is caused by entropic effects, and for channel R2a, both entropic and energetic factors should be responsible for the curved plot. Also, it is clear that there is no tunneling for these three reactions due to the negative adiabatic energy barriers. While for R1b-1 (see Figure 4d) and R1b-2 and R2b (see Figure S2 a-b), the TST rate constants are almost the same as the ICVT ones, i.e. the varational effect is small or negligible, but the tunneling contributions are large at low temperatures and become negligible as temperature increases. For example, for R1b-1, the k(ICVT/SCT)/k(ICVT) values are 11.3 at 200 K, 1.57 at 500 K, and 1.12 at 1000 K. The tunneling effect results in the curved Arrhenius plots for these reactions of H-abstraction from the -CH_2- group.

The overall rate constant of each conformer is the sum of the individual ICVT/SCT result, that is, $k_1 = k_{1a} + k_{1b} = (k_{1a\text{-}1} + k_{1a\text{-}2}) + (k_{1b\text{-}1} + k_{b\text{-}2})$ and $k_2 = k_{2a} + k_{2b}$. It is found that the rate constants k_{1a} and k_{2a} of the H-abstraction from the -CHO group are about 4-1 orders of magnitude larger than the rate constants, k_{1b} and k_{2b}, of the hydrogen-abstractions from the -CH_2- group in the whole temperature range of 200-2000 K. Accordingly, the overall rate constant of each conformer (k_1 or k_2) is almost equal to, k_{1a} or k_{2a}, while the contributions of those H-abstraction channels from the -CH_2- group to the reaction can be negligible at whatever temperature.

The total rate constant (k_T) for the title reaction CF_3CH_2CHO + OH → products can be obtained by the following expression:

$$\begin{aligned} k_T &= \omega_1 k_1 + \omega_2 k_2 \\ &= \omega_1 (k_{1a\text{-}1} + k_{1a\text{-}2} + k_{1b\text{-}1} + k_{b\text{-}2}) + \omega_2 (k_{2a} + k_{2b}) \\ &= k_{1T} + k_{2T} \end{aligned} \quad \text{(E1)}$$

where ω_1 and ω_2 are the weight factors of t- and c-CF_3CH_2CHO calculated from the Boltzmann distribution function. The theoretical rate constants and available experi-

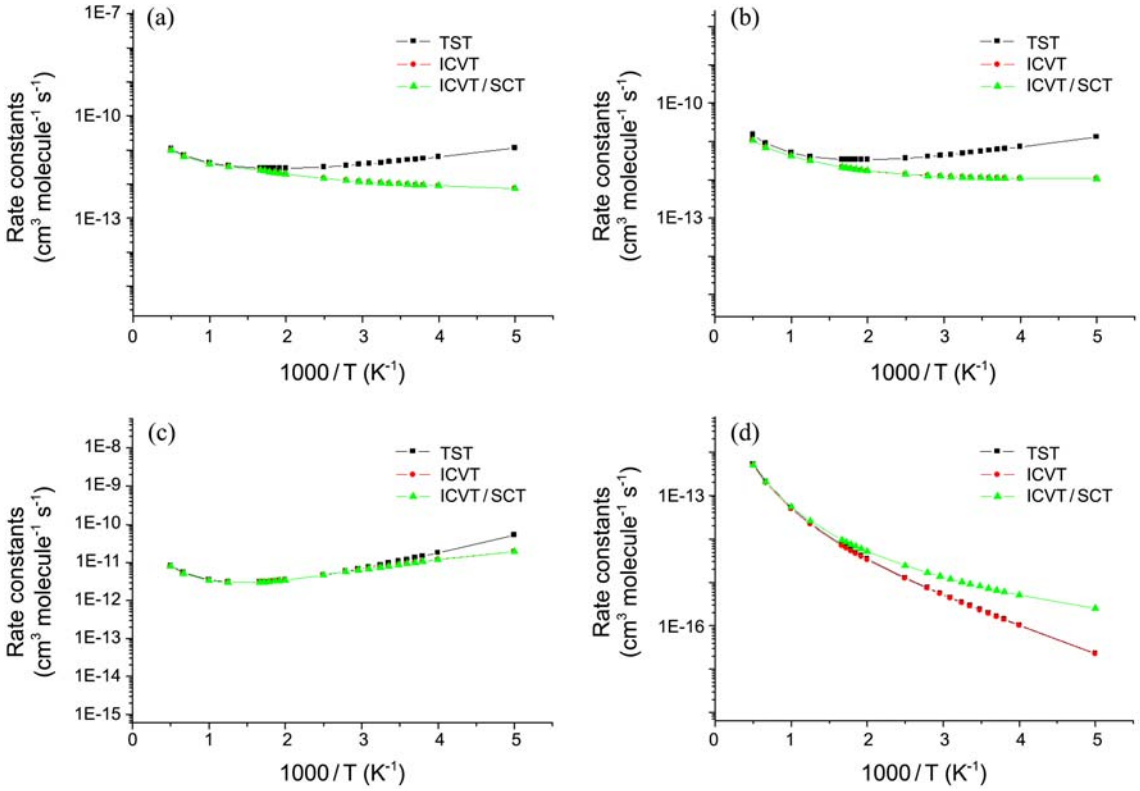

Figure 4. The TST, ICVT, and ICVT/SCT rate constants calculated at the MCG3-MPWB//M06-2X/aug-cc-pVDZ level *versus* 1000/*T* between 200 and 2000 K: (a) for R1a-1, (b) for R1a-2, (c) for R2a, and (d) for R1b-1.

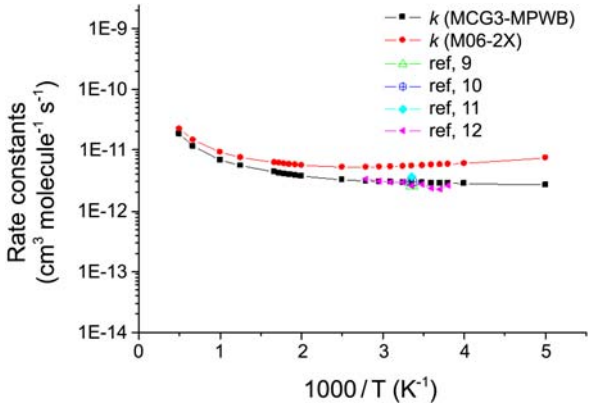

Figure 5. The total rate constants k_T and available experimental values (in cm^{3}molecule^{-1} s^{-1}) *versus* 1000/*T* between 200 and 2000 K for the reaction of CF_3CH_2CHO + OH.

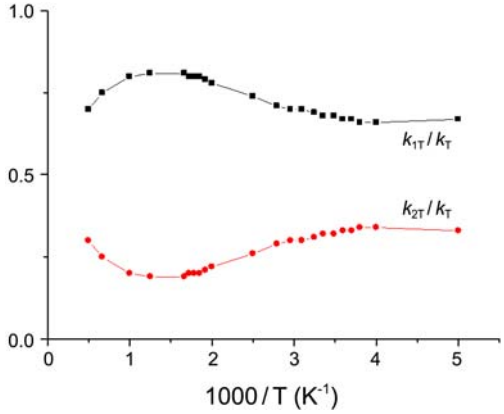

Figure 6. Plot of the contributions of *t*-CF_3CH_2CHO and *c*-CF_3CH_2CHO to the reaction *versus* 1000/*T* between 200 and 2000 K.

mental data are displayed in Figure 5. It is shown that the calculated dual-level ICVT/SCT rate constants agree quite well with the experimental values in the measured temperature range. For example, the k_T(ICVT/SCT) at T = 298 K is 2.87×10^{-12} cm^3 molecule^{-1} s^{-1}, which is in excellent agreement with the experimental values of $(2.96 \pm 0.04) \times 10^{-12}$,[9] $(2.57 \pm 0.44) \times 10^{-12}$ [10] and $(2.59 \pm 0.50) \times 10^{-12}$ [11] cm^3 molecule^{-1} s^{-1}, while slightly lower than the determined data, $(3.6 \pm 0.3) \times 10^{-12}$ [12] cm^3 molecule^{-1} s^{-1}; in the temperature range 263-358 K, the deviation of the calculated and experimental rate constants by Antiñolo *et al.*[11] is within a factor of 0.3. In addition, although k_{2a} shows negative temperature dependence below 820 K, the total rate constants of the CF_3CH_2CHO + OH reaction exhibit a slightly positive temperature dependence.

From expression E1, the degree of each conformer contributing to the total rate constant can be evaluated easily, for example, the values of ω_1 are 0.96 at 200 K and 0.58 at 2000 K. The contributions of *t*- and *c*-CF_3CH_2CHO, i.e., k_{1T}/k_T and k_{2T}/k_T, to the title reaction are plotted in Figure 6. It is seen that the k_{1T}/k_T ratio changes from 0.67 to 0.7 within 200-2000 K, which means that the conformer *t*-CF_3CH_2CHO provides a major contribution to the title reaction, but the contributions of *c*-CF_3CH_2CHO cannot be neglected and

should be taken into account over the whole temperature range.

Since no experimental data are available at higher temperatures, for kinetic modeling application as well as providing theoretical prediction for future experimental study, the total rate constants are fitted to modified Arrhenius equation. The four-parameter rate-temperature expression proposed by Truhlar *et al.*[37] is approved to give small fitting error and have the correct low-temperature asymptotic behavior for activation energy and rate constant. The corresponding rate constant expression and activation energy are

$$k_T = A(T/300)^n \exp\left[\frac{-E(T+T_0)}{R(T^2+T_0^2)}\right] \quad \text{(E2)}$$

$$E_a = E\,\frac{T^4+2T_0T^3-T_0^2T^2}{(T^2+T_0^2)^2} + nRT \quad \text{(E3)}$$

where A, n, E, and T_0 are fitting parameters, and R is the gas constant. For the present system, we used this model in fitting rate constants within 200-2000 K, and the four-parameter rate-temperature expression is given as follows (in cm^3 $molecule^{-1}$ s^{-1}),

$$k_T = 3.18 \times 10^{-18} T^{2.0} \exp\left[\frac{638.2(T+240.3)}{T^2+5.8\times10^4}\right]$$

In addition from E2, the estimated activation energy between 263 and 358K is 0.65 kcal mol^{-1}, in excellent agreement with the experimental value of 0.62 kcal mol^{-1}.[11]

Conclusions

In this paper, the mechanism and kinetics of the CF_3CH_2CHO + OH reaction have been studied by dual-level direct dynamics method at the MCG3-MPWB//M06-2X/aug-cc-pVDZ level. *Trans* and *cis* conformers of CF_3CH_2CHO were located by rotation of the -CHO group, and the former is about 1.2 kcal mol^{-1} more stable than the latter. For each conformer, the hydrogen atoms can be abstracted from the -CHO group and $-CH_2-$ group, respectively. The rate constants of each H-abstraction channel were calculated by using improved canonical variational transition-state theory (ICVT) with the small-curvature tunneling (SCT) correction over a wide temperature range of 200-2000 K. The present calculations show that the hydrogen abstractions from the -CHO group (R1a and R2a) are the predominant channels over the entire temperature range, while the contributions of H-abstractions from the $-CH_2-$ group are negligible. The ICVT/SCT rate constants and estimated activation energy are in good agreement with the available experimental values. Furthermore, the enthalpies of formation of reactant and product radicals were estimated by using isodemic reactions.

Acknowledgments. We thank Professor Donald G. Truhlar for providing the POLYRATE 9.7 program. This work is supported by the National Nature Science Foundation of China (20973077, 20303007) and the Program for New Century Excellent Talents in University (NCET).

References

1. Liu, R.; Huie, R. E.; Kurylo, M. J. *J. Phys. Chem*. **1990**, *94*, 3247.
2. Hsu. K. J.; DeMore, W. B. *J. Phys. Chem*. **1995**, *99*, 1235.
3. Talhaoui, A.; Louis, F.; Devolder, P.; Meriaux, B.; Sawerysyn, J. P. *J. Phys. Chem*. **1996**, *100*, 13531.
4. Sekiya, A.; Misaki, S. In *Proceedings of the International Conference on Ozone Protection Technologies*; Baltimore: Maryland, 12-13 November, 1997; p 26.
5. Kambanis, K. G.; Lazarou, Y. G.; Papagiannakopoulos, P. *Air Pollution esearch report 66, "Polar Stratospheric Ozone 1997"*; European Commission: Belgium, 1998; p 557.
6. Kissa, E., Schick, M. J., Fowkes, F. M., Eds.; *Fluorinated Surfactants, Synthesis, Properties, and Applications*; Marcel Dekker: New York, 1994.
7. Sellevåg, S. R.; Nielsen, C. J.; Sovde, O. A.; Myhre, G.; Sundet, J. K.; Stordal, F.; Isaksen, I. S. *Atoms. Environ*. **2004**, *38*, 6725.
8. Hurley, M. D.; Wallington, T. J.; Sulbaek Andersen, M. P.; Ellis, D. A.; Martin, J. W.; Mabury, S. A. *J. Phys. Chem. A*. **2004**, *108*, 1973.
9. Kelly, T.; Bossoutrot, V.; Magneron, I.; Wirtz, K.; Treacy, J.; Mellouki, A.; Sidebottom, H.; Le Bras, G. *J. Phys. Chem. A* **2005**, *109*, 347.
10. Hurley, M. D.; Misner, J. A.; Ball, J. C.; Wallington, T. J.; Ellis, D. A.; Martin, J. W.; Mabury, S. A., Sulbaek Andersen, M. P. *J. Phys. Chem. A* **2005**, *109*, 9816.
11. Antiñolo, M.; Jiménez, E.; Notario, A.; Martínez, E.; Albaladejo, J. *Atoms. Chem. Phys*. **2010**, *10*, 1911.
12. Sellevåg, S. R.; Kelly, T.; Sidebottom, H.; Nielsen, C. J. *Phys. Chem. Chem. Phys.* **2004**, *6*, 1243.
13. Truhlar, D. G. In *The Reaction Path Chemistry*: *Current Approaches and Perspectives*; Heidrich, D., Kluwer, D., Eds.; The Netherlands, 1995; p 229.
14. Truhlar, D. G.; Garrett, B. C.; Klippenstein, S. J. *J. Phys. Chem.* **1996**, *100*, 12771.
15. Hu, W. P.; Truhlar, D. G. *J. Am. Chem. Soc*. **1996**, *118*, 860.
16. Zhao, Y.; Truhlar, D. G. *Theor. Chem. Acc.* **2008**, *120*, 215.
17. Zhao, Y.; Truhlar, D. G. *J. Phys. Chem. A* **2005**, *109*, 4209.
18. Truhlar, D. G.; Garrett, B. C. *Acc. Chem. Res*. **1980**, *13*, 440.
19. Truhlar, D. G.; Lsaacson, A. D.; Garrett, B. C. *The Theory of Chemical Reaction Dynamics*; Bear, M., Ed.; CRC: Boca Raton, FL, 1985; p 65.
20. Truhlar, D. G.; Garrett, B. C. *Anmu. Rev. Phys. Chem.* **1984**, *35*, 159.
21. Chuang, Y. Y.; Corchado, J. C.; Truhlar, D. G. *J. Phys. Chem. A* **1999**, *103*, 1140.
22. IUPAC. Available from: http://www.iupac.org/reports/1999/7110minkin/i.html.
23. Montgomery, J. A., Jr.; Frisch, M. J.; Ochterski, J. W.; Petersson, G. A. *J. Chem. Phys.* **2000**, *112*, 6532.
24. Ochterski, J. W.; Petersson, G. A.; Montgomery, A. J., Jr. *J. Chem. Phys.* **1996**, *104*, 2598.
25. Zhao, Y.; Truhlar, D. G. *MLGAUSS-Version 2.0*; University of Minnesota: Minneapolis, 2005.
26. Frisch, M. J.; Truck, G. W.; Schlegel, H. B.; Scuseria, G. E.; Robb, M. A.; Cheeseman, J. R.; Zakrzewski, V. G.; Montgomery, J. A.; Jr.; Stratmann, R. E.; Burant, J. C.; Dapprich, S.; Millam, J. M.; Daniels, A. D.; Kudin, K. N.; Strain, M. C.; Farkas, O.; Tomasi, J.; Barone, V.; Cossi, M.; Cammi, R.; Mennucci, B.; Pomelli, C.; Adamo, C.; Clifford, S.; Ochterski, J.; Petersson, G. A.; Ayala, P. Y.; Cui, Q.; Morokuma, K.; Malick, D. K.; Rabuck, A. D.; Raghavachari, K.; Foresman, J. B.; Cioslowski, J.; Ortiz, J. V.; Boboul, A. G.; Stefnov, B. B.; Liu, G.; Liaschenko, A.; Piskorz, P.; Komaromi, L.; Gomperts, R.; Martin, R. L.; Fox, D. J.; Keith, T.; Al-Laham, M. A.; Peng, C. Y.; Nanayakkara, A.; Gonzalez, C.; Challacombe, M.; Gill, P. M. W.; Johnson, B.; Chen, W.; Wong,

M. W.; Andres, J. L.; Gonzalez, C.; Head-Gordon, M.; Replogle E. S.; Pople, J. A. *GAUSSIAN 03*, Revision A.1, Guassian, Inc., Pittsburgh, PA, 2003.
27. Gaussian 09, Revision, A. L.; Frisch, M. J.; Trucks, G. W.; Schlegel, H. B.; Scuseria, G. E.; Robb, M. A.; Cheeseman, J. R.; Scalmani, G.; Barone, V.; Mennucci, B.; Petersson, G. A.; Nakatsuji, H.; Caricato, M.; Li, X.; Hratchian, H. P.; Izmaylov, A. F.; Bloino, J.; Zheng, G.; Sonnenberg, J. L.; Hada, M.; Ehara, M.; Toyota, K.; Fukuda, R.; Hasegawa, J.; Ishida, M.; Nakajima, T.; Honda, Y.; Kitao, O.; Nakai, H.; Vreven, T.; Montgomery, J. A., Jr.; Peralta, J. E.; Ogliaro, F.; Bearpark, M.; Heyd, J. J.; Brothers, E.; Kudin, K, N.; Staroverov, V. N.; Kobayashi, R.; Normand, J.; Raghavachari, K.; Rendell, A.; Burant, J. C.; Iyengar, S. S.; Tomasi, J.; Cossi, M.; Rega, N.; Millam, N. J.; Klene, M.; Knox, J. E.; Cross, J. B.; Bakken, V.; Adamo, C.; Jaramillo, J.; Gomperts, R.; Stratmann, R. E.; Yazyev, O.; Austin, A. J.; Cammi, R.; Pomelli, C.; Ochterski, J. W.; Martin, R. L.; Morokuma, K.; Zakrzewski, V. G.; Voth, G. A.; Salvador, P.; Dannenberg, J. J.; Dapprich, S.; Daniels, A. D.; Farkas, O.; Foresman, J. B.; Ortiz, J. V.; Cioslowski, J.; Fox, D. J.; Gaussian, Inc., Wallingford CT 2009.
28. Corchado, J. C.; Chuang, Y. Y.; Fast, P. L.; Hu, W. P.; Liu, Y. P.; Lynch, G. C.; Nguyen, K. A.; Jackels, C. F.; Ramos, A. F.; Ellingson, B. A.; Lynch, B. J.; Melissas, V. S.; Villa, J.; Rossi, I.; Coitino, E. L.; Pu, J.; Albu, T. V.; Steckler, R.; Garrett, B. C.; Isaacson, A. D.; Truhlar, D. G. POLYRATE, version 9.7; University of Minnesota: Minneapolis, MN, 2007.
29. Garrett, B. C.; Truhlar, D. G.; Grev. R. S.; Magnuson, A. W. *J. Phys. Chem.* **1980**, *84*, 1730.
30. Lu, D. H.; Truong, T. N.; Melissas, V. S.; Lynch, G. C.; Liu, Y. P.; Grarrett, B. C.; Steckler, R.; Issacson, A. D.; Rai, S. N.; Hancock, G. C.; Lauderdale, J. G.; Joseph, T.; Truhlar, D. G. *Comput. Phys. Commun.* **1992**, *71*, 235.
31. Liu, Y. P.; Lynch, G. C.; Truong, T. N.; Lu, D. H.; Truhlar, D. G.; Grarrett, B. C. *J. Am. Chem. Soc*. **1993**, *115*, 2408.
32. Truhlar, D. G. *J. Comput. Chem*. **1991**, *12*, 266.
33. Chuang, Y. Y.; Truhlar, D. G. *J. Chem. Phys*. **2000**, *112*, 1221.
34. Lide, D. R. *CRC Handbook of Chemistry and Physics*, 80th ed.; CRC Press: New York, 1999.
35. NIST Chemistry Webbook, Linstrom, P. J., Mallard, W. G., Eds.; NIST Standard Reference Database Number 69, http://webbook. Nist.Gov/chemistry.
36. Wu, E. C.; Rodgers, A. S. *J. Phys. Chem*. **1974**, *78*, 2315.
37. Zhang, J. J.; Truhlar, D. G. *Phys. Chem. Chem. Phys*. **2010**, *12*, 7782.
38. Shimanouchi, T. *Tables of Molecular Vibrational Frequencies Consolidated*; National Bureau of Standandard; U. S. Government Pring Office: Washington, D. C., 1972; Vol. 1.